Radar observations of individual rain drops in the free atmosphere

Jerome M. Schmidt[a,1], Piotr J. Flatau[b], Paul R. Harasti[a], Robert D. Yates[c], Ricky Littleton[c], Michael S. Pritchard[b], Jody M. Fischer[d], Erin J. Fischer[d], William J. Kohri[e], Jerome R. Vetter[e], Scott Richman[c], Dariusz B. Baranowski[f], Mark J. Anderson[g], Ed Fletcher[h], and David W. Lando[g]

[a]Marine Meteorology Division, Naval Research Laboratory, Monterey, CA 93943; [b]Scripps Institution of Oceanography, University of California, San Diego, CA 92093; [c]L-3 Interstate Electronics Corp., Anaheim, CA 92803; [d]Weather Modification INC, Fargo, ND 38102; [e]The Johns Hopkins University Applied Physics Laboratory, Laurel, MD 20723; [f]Institute of Geophysics, University of Warsaw, Pasteura 7, Warsaw 02093, Poland; [g]Naval Surface Warfare Center Dahlgren Division, Dahlgren, VA 22448; and [h]Radar Technology Specialists Corp., Palos Verdes, CA 90274

Edited by Mark H. Thiemens, University of California San Diego, La Jolla, CA, and approved April 20, 2012 (received for review October 28, 2011)

Atmospheric remote sensing has played a pivotal role in the increasingly sophisticated representation of clouds in the numerical models used to assess global and regional climate change. This has been accomplished because the underlying bulk cloud properties can be derived from a statistical analysis of the returned microwave signals scattered by a diverse ensemble comprised of numerous cloud hydrometeors. A new Doppler radar, previously used to track small debris particles shed from the NASA space shuttle during launch, is shown to also have the capacity to detect individual cloud hydrometeors in the free atmosphere. Similar to the traces left behind on film by subatomic particles, larger cloud particles were observed to leave a well-defined radar signature (or streak), which could be analyzed to infer the underlying particle properties. We examine the unique radar and environmental conditions leading to the formation of the radar streaks and develop a theoretical framework which reveals the regulating role of the background radar reflectivity on their observed characteristics. This main expectation from theory is examined through an analysis of the drop properties inferred from radar and in situ aircraft measurements obtained in two contrasting regions of an observed multicellular storm system. The observations are placed in context of the parent storm circulation through the use of the radar's unique high-resolution waveforms, which allow the bulk and individual hydrometeor properties to be inferred at the same time.

microphysics | convection | cumulonimbus | backscatter

One of the greatest uncertainties in long-term climatic prediction stems from the numerical representation or parameterization of radiatively important cloud systems in climate models (1). As the design of the cloud parameterizations themselves are based on observed cloud structure and dynamics, a concerted effort has been underway to improve the monitoring of global cloud structure through atmospheric remote sensing means (1, 2). The enhanced monitoring of the bulk cloud properties such as the reflectivity, Doppler-derived flow, or particle phase has led to a fundamental increase in the understanding of the underlying cloud structure and dynamics as well as provided a means in which to assess the design and performance of the cloud schemes used in general weather and climate prediction systems alike (3–11). Understandably, microwave radar studies of individual hydrometeors has remained a more elusive undertaking with the vast majority of studies conducted under highly controlled settings in which single isolated particles are suspended in wind tunnels or tethered to balloons (12–14). Nevertheless, these studies have revealed considerable insights on the shape, oscillatory behavior, and terminal velocity of drops suspended in a free airstream which govern the particle collection and collision rates that ultimately control the onset and fallout of precipitation-sized particles from a wide variety of the planet's cloud systems.

The ability to detect and characterize the properties of individual cloud hydrometeors formed within the free atmosphere could arguably be considered the next significant step in remote sensing, particularly if the bulk properties of the cloud system could be ascertained at the same time. This hybrid approach is examined here using the high-resolution 3 MW, dual-polarization, C-band, Pulsed Doppler Mid-Course Radar (MCR) operated in the Cape Canaveral region of Florida by the US Navy. The ability of the MCR to simultaneously record the bulk and individual drop properties within a given cloud system stems from the properties of two linear frequency modulated wave forms which are alternatively transmitted with a pulse repetition frequency (PRF) of 160.1 Hz. Each waveform has a narrow 0.22 degree beam width and a 6 dB width range resolution of either 37 m or 0.546 m (referred to as the narrow and wideband wave forms, respectively, throughout the text). This combination of signal attributes leads to the remarkably small pulse volumes of the wideband (as fine as $\sim 14\ \mathrm{m}^3$ at the range of 2000 m used in this study), which make it possible to sample individual cloud hydrometeors.

We examine the properties of a series of peculiar, nearly linear high-reflectivity echo patterns that appear in the wideband data, which are henceforth referred to as "streaks" in light of the previous wind tunnel observations of (15). An analysis of the factors contributing to their detection and observed characteristics is simplified by the fact that the diameters (D_i) of the individual streak particles are observed to lie within the Rayleigh scattering regime [$D_i < \lambda/16 < 3.3$ mm given the MCR's 0.05306-m wideband wavelength (λ)], where the radar reflectivity factor in a unit volume of air (Z) can be expressed as $Z = \Sigma D_i^{\,6}$. When a single large particle (the streak) enters a radar sample volume filled with numerous smaller drops, this strong D^6 dependency on Z (hereafter referred to more simply as the reflectivity) can be exploited in a manner which reveals the conditions under which certain particles stand out as streaks against a given "background" reflectivity field.

This main theme of the paper is pursued through a series of plots which reveal the nature of the streaks observed within two regions of the same storm complex exhibiting significant differences in their overall reflectivity structure. Three independent techniques for ascertaining the drop velocity and diameter

Author contributions: J.M.S., P.J.F., P.R.H., J.R.V., M.J.A., E.F., and D.W.L. designed research; J.M.S., P.J.F., P.R.H., R.D.Y., M.S.P., and D.B.B. performed research; P.R.H., R.D.Y., R.L., J.M.F., E.J.F., W.J.K., J.R.V., S.R., and E.F. contributed new reagents/analytic tools; R.L. operated MCR radar; M.S.P. (student participant) assisted with surface instrumentation; J.M.F. and E.J.F. obtained in situ cloud data; W.J.K. released rawinsondes used in the analysis; R.D.Y. and S.R. processed all MCR radar data; D.B.B. (student participant) assisted with surface instrumentation and aircraft observations; E.F. primary radar designer and day-to-day radar coordinator; J.M.S., P.J.F., P.R.H., and R.D.Y. analyzed data; and J.M.S. and P.J.F. wrote the paper.

The authors declare no conflict of interest.

This article is a PNAS Direct Submission.

[1]To whom correspondence should be addressed. E-mail: schmidt@nrlmry.navy.mil.

This article contains supporting information online at www.pnas.org/lookup/suppl/doi:10.1073/pnas.1117776109/-/DCSupplemental.

characteristics from the streak observations in each region are obtained by computing: (*i*) the velocity from the measured streak slope obtained from the radar-derived time-height reflectivity plots; (*ii*) the diameter from the magnitude of the along-streak radar reflectivity; and (*iii*) the velocity from the Doppler phase shift using the techniques discussed by (16). The accurate diameter-dependent rain drop terminal velocity (V_T) formulas of (17) are then used to provide a linkage between the independent particle diameter and velocity estimates. By plotting the derived streak diameters obtained in each region versus their observed background reflectivity field, we then arrive at the result which reveals the underlying role of the background reflectivity in governing the size of the observed streak particles.

Results

To provide a feel for the sensitivity of the MCR radar and, in fact, to show that it is capable of detecting a single rain drop as claimed, we first derive an estimate of the smallest detectable particle at a given range of interest in the following form:

$$D = \left\{ \frac{\mathrm{SIR}(\mathrm{ZNR}+1)R^4}{\mathrm{LG}} \frac{\lambda^4}{\pi^5 |K_p|^2} \right\}^{\frac{1}{6}}, \qquad \textbf{[1A]}$$

where D is the particle diameter (in millimeters), λ is the radar wavelength, LG is the MCR loop gain expressed as a power ratio of the signal power to noise power and has a value of 10^{27} m^2 (or 270 dB), K_p is the dielectric constant of the particle, R is the range to the particle in meters, and the signal-to-noise ratio [$\mathrm{SNR} = \mathrm{SIR}(\mathrm{ZNR}+1)$] is written in terms of the combined effects of the particle (SIR) and background (ZNR) signal-to-noise power ratios. In deriving Eq. **1***A*, we make the assumption that the particle in question satisfies the Rayleigh approximation and that the quantity $\mathrm{LG}/(1+\mathrm{ZNR})$ can be interpreted as the radar loop gain in the presence of the interfering background return. Note that Eq. **1***A* takes on the more standard textbook form when ZNR approaches zero and the ratio $R^4\mathrm{SIR}/\mathrm{LG}$ is replaced by the usual radar backscatter cross-sectional area (σ).

When the background signal-to-noise power ratio is large, Eq. **1***A* can also be written as follows:

$$D = \left\{ \frac{\mathrm{SIR}(\mathrm{ZNR}^{-1}+1)R^2 Z_b |K_\mathrm{b}|^2 V_1}{|K_p|^2} \right\}^{\frac{1}{6}}, \qquad \textbf{[1B]}$$

where V_1 (m^3/km^2) is the illuminated volume normalized to R^2 (i.e., the volume at a range of 1 meter), which depends on the antenna beam widths and range resolution; Z_b is the background reflectivity in units of mm^6 m^{-3}; and K_b is the dielectric constant of the background particles. These two expressions are equivalent, but Eq. **1***A* can be used to show the limits for D as ZNR approaches zero (in which case $\mathrm{SNR} \sim \mathrm{SIR}$), while Eq. **1***B* can be used to show the limit for D when $\mathrm{ZNR} \gg 1$. We also see from Eq. **1***B* that the minimum detectable particle of diameter D is directly proportional to the range to the particle, the value of the background reflectivity, and the water phase of both the particle and background.

Both forms of Eq. **1** are useful in that they indicate that the value of minimum detectable diameter needs to increase when $\mathrm{ZNR} \gg 1$ in order for that particle to be detected above and beyond that of the background noise. Theoretically, $\mathrm{SNR} = 1$ is the threshold at which the particle has a power just equal to the noise; however, a SNR up to a value of approximately 6 dB is often required in practice in order for the particle to be unambiguously resolved above the noise level. As a concrete example, using a dielectric constant of 1.0, a range of 2,000 m, and SNR values of 0 and 6 dB, we arrive at minimum diameter estimates representative of readily observable small rain drops (0.276 and 0.35 mm for SNR values of 0 and 6 dB, respectively).

The two main expectations from Eq. **1***A* are that the background reflectivity regulates the size of the streak particles and that the MCR can detect individual hydrometeors generating streaks provided that they are observed relatively close to the radar. To test these two main tenets of Eq. **1**, we examine the radar data derived from two high-range resolution (0.5 m) wideband analysis domains (labeled B1 and B2 in Fig. 1) which sampled the lower portion of a weak multi-cellular storm complex that was observed to produce streaks as it passed directly over the vertically pointed MCR during the afternoon of August 27, 2010. The temporally averaged view of this storm system derived from the perspective of the lower range resolution (37 m) narrowband wave form reveals that the MCR sampled two shallow convective cells (labeled A and B) in excess of 20 dBZ during the 1-h measurement period as well as an intervening gap between cells where the observed reflectivity was found to be considerably lower. In the vicinity of the B1 and B2 analysis domains, the reflectivity differential approached 40 dBZ, and this was thus deemed to be of sufficient spread in order to test the predictions of Eq. **1**.

The available in situ aircraft and radar measurements shown in Fig. 1 suggest that the hydrometeors entering these two analysis domains originated further aloft as ice particles prior to melting and settling into the lower portions of the storm as liquid particles within the series of narrow precipitation streamers that are seen to stem from the area of the radar reflectivity bright band evident near 4.6 km. Note that the reflectivity values within the precipitation streamers quickly fade with distance below the melting level, particularly in the gap region between the two dominant cells, indicating either a transport of the drops out of the MCR's time-height observational plane by the environmental flow and/or the onset of significant evaporation. The latter possibility is supported by the dry environmental conditions observed below the melting level by both the aircraft (Fig. 1) and a rawinsonde ascent which occurred in the prestorm environment (Fig. S1). The measured mean layer values near 70% indicate that the rain drops would have been susceptible to considerable evaporation in the intervening layers prior to entering the B1 and B2 analysis domains (18, 19). This likely would have contributed to a significant reduction in the particle concentration and size as the particles settled from flight level into the lower reaches of the

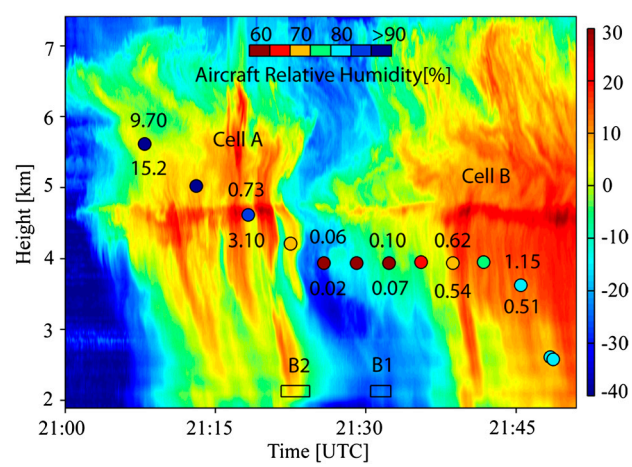

Fig. 1. Time-height cross-section of the MCR narrowband reflectivity (in dBZ and shaded) between 2100 and 2200 UTC August 27, 2010. The black boxes labeled B1 and B2 denote regions of the cloud system examined with the high-resolution wide-band waveform. The colored circles denote the altitude and relative humidity with respect to water (in percent) observed by the research aircraft when directly over the MCR. The color bar for the relative humidity resides near the top of the image. The labels found above and below the colored circles represent the total droplet concentrations from the FSSP [cm^{-3}] and the 2DC [L^{-1}] probes, respectively. The cells labeled A and B denote the location of the primary cells discussed in the text.

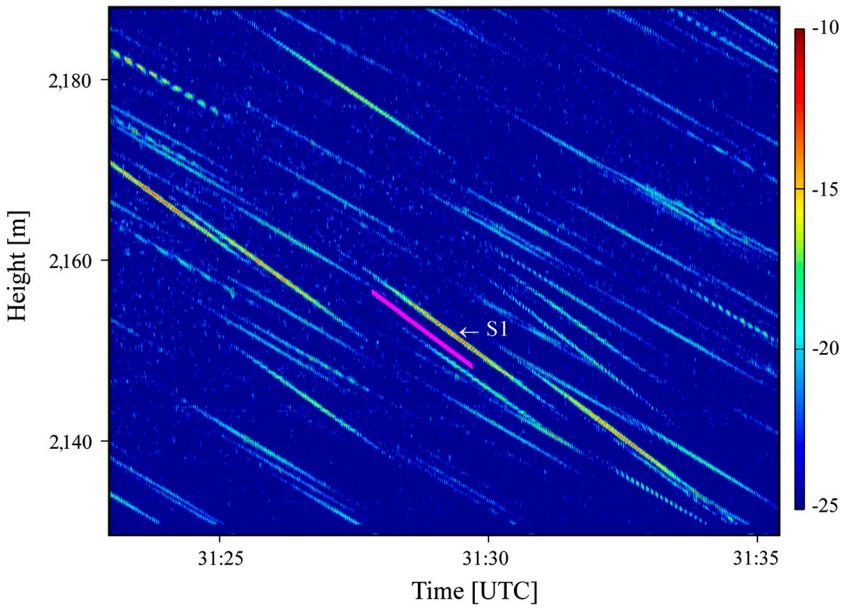

Fig. 2. Time-height plot of the MCR wideband reflectivity (dBZ) shown for the analysis box labeled B1 in Fig 1. The location of the displayed domain is depicted by the white box shown in Fig. S2. The "streak" labeled S1 is singled out for additional analyses in the text. The bold magenta line segment depicts the power spectra derived velocity estimate of the S1 particle. The labeling on the abscissa represents the time in minutes and seconds (mm:ss) after 2100 UTC.

storm, particularly in the gap region containing the B1 analysis domain which lacked the more persistent precipitation streamers observed in either of the two main convective cells.

While the temporally averaged narrowband reflectivity structure evident in Fig. 1 exhibits considerable detail, there is nothing in the plot to indicate that the MCR is capable of detecting individual drops as previously claimed. This perception changes dramatically, though, when the colocated wideband data is viewed at the full native temporal and 0.5 m range resolution of the MCR (Figs. 2 and 3). These images from the B1 and B2 analysis domains (see Figs. S2 and S3 for the locations of these domains) reveal a remarkably rich reflectivity structure that consists of distinct and nearly parallel linear sloping reflectivity maxima or "streaks" that stand out against the weaker and more uniform background reflectivity field. Note that each streak in Figs. 2 and 3 slopes downward in time from left to right across the plots, indicating inbound "targets" that are moving toward the vertically pointed MCR at relatively constant speeds. One also clearly begins to see the discrete nature of the streaks as well as the variability in their various attributes such as the slope, concentration, length, and magnitude of the along-streak radar return.

As initially anticipated from Eq. **1***A*, and as suggested above from the available radar and in situ aircraft data shown in Fig. 1, the variability in the observed streak structure provides the first indication that the underlying particles in these two regions of the storm fall into two distinctly different size categories. A more

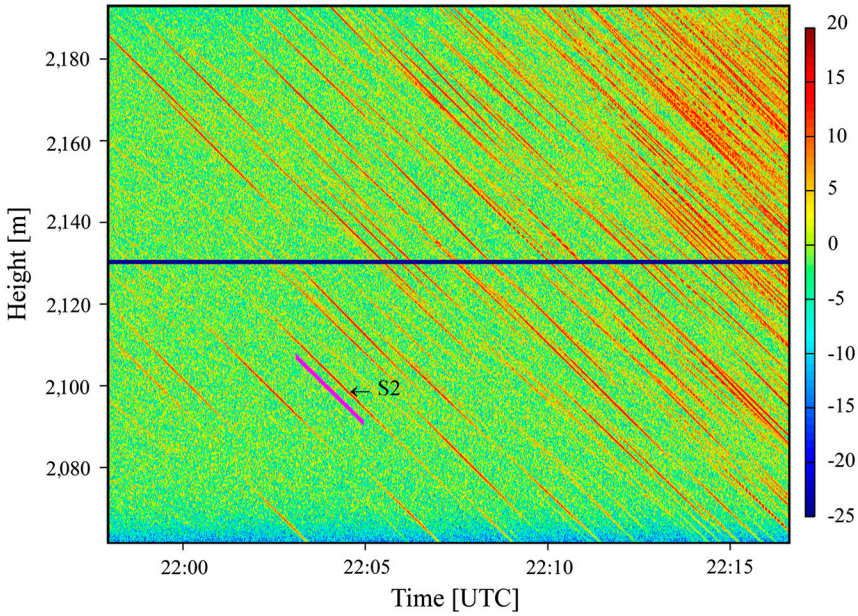

Fig. 3. As in Fig. 2 except that the data represents the analysis domain labeled B2 in Fig. 1. The domain location is depicted by the white box shown in Fig. S3. The "streak" labeled S2 is singled out for additional analyses in the text. The bold magenta line depicts the power spectra derived velocity estimate of the S2 particle.

quantitative comparison of the streak properties in each region can be conducted from an analysis of the particle diameter and/or velocity obtained from three independent methods derived from the measured streak slope, reflectivity magnitude, and Doppler-derived velocity (Fig. 4 and Fig. S4). The data reveal that the S2 particle was nearly three times larger and was falling at nearly twice the velocity of the S1 particle (Fig. S4). The power spectra analysis shown in Fig. 4 also strongly suggests that these two streaks were caused by a single dominant particle falling with an unambiguous velocity of −4.4 and −8.8 ms^{-1}, respectively (Table S1). Other minor peaks evident in the power spectrum at or just below the noise threshold [computed using the method of (20)] are attributed to radar receiver noise and the smaller particles comprising the background reflectivity in each case. Using the analysis of (17), the Doppler-derived velocity values translate into particle diameter estimates of 1.0 and 2.9 mm for the S1 and S2 streaks, respectively (Table S1). These diameter and velocity estimates are nearly identical to those obtained from the slope method and are only slightly greater (by less than 0.2 mm and 0.4 ms^{-1}, respectively) than those derived from the reflectivity measurements using Eq. **1***A* (Table S1). The reduction in the particle size estimates obtained from the reflectivity suggests that the particles either did not pass directly through the center of the beam (resulting in a reduction of the diameter estimate derived from the measured reflectivity) or were possibly embedded in a weak downdraft at the time of the observations.

When examining the reflectivity-based characteristics of individual particles, it becomes important to ascertain the possible impact on the derived particle diameter and velocity caused by variations in the particle's position, orientation, or shape within the beam. The lower frequency parabolic trend for each streak evident in Fig. S4 (given by the fitted bold dashed line in each plot) can be tied to the horizontal movement of the particle across the beam caused by the weak environmental flow (Fig. S5), and it is this factor which impacts the streak length evident in Figs. 2 and 3. The higher-frequency fluctuations that are also evident are more difficult to ascertain, but have been noted to occur in highly controlled wind tunnel studies (12, 13, 15) where they have been attributed to naturally occurring drop oscillations of the type examined by (21, 22). As alluded to by (12, 23), additional impacts on the characteristics of the oscillations in the real atmosphere can be expected to result from turbulent motion of the air, electrical effects, or the presence of other drops.

Using the slope method, all remaining streaks discernible in the radar volumes containing the B1 and B2 analysis boxes were analyzed to produce the histogram plots shown in Fig. 5. The analysis confirms the distinct nature of the drop populations which are seen to conveniently fall into either the regime2 (B1) or regime3 (B2) drop size regimes studied by (17, 24). As might also be inferred from the nearly parallel nature of the streaks evident in Figs. 2 and 3, the diameter and velocity range for these particles cover a rather small velocity and size range. The derived B1 size distribution had a sharp peak near 0.75 mm and a main velocity peak near −3.5 ms^{-1}, while the larger B2 particles exhibited a peak in the size distribution near 3 mm and contained drops with terminal velocities generally in excess of −7 ms^{-1}. Note also that the minimal detectable diameter for the B1 particles (600 μm) is nearly twice that expected at this range, while that of the B2 particles is some six times greater. As we see in the *Discussion*, these differences reflect the controlling influence of the background reflectivity on the lowest detectable particle size.

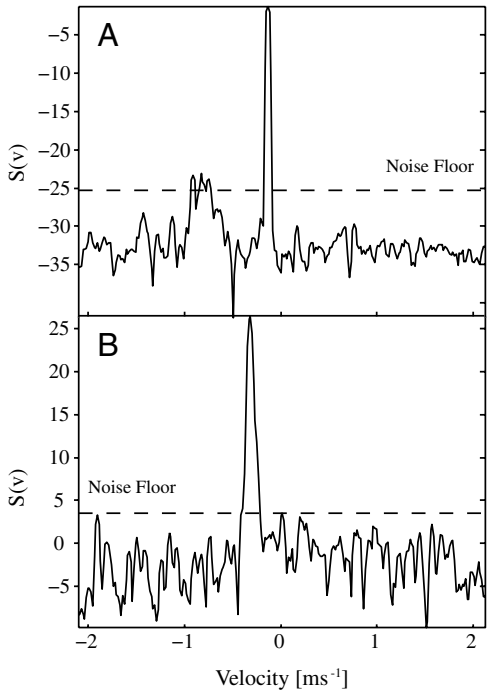

Fig. 4. The Doppler-derived power spectra ($10\log[mm^6\,m^{-3}\,(ms^{-1})^{-1}]$) for: (*A*) the streak labeled S1 in Fig. 2, and (*B*) the streak labeled S2 in Fig. 3. Following (20), the plotted spectra and noise floor estimates [denoted by the horizontal dashed lines in (*A*) and (*B*)] are computed from a running 3-point average of the raw spectra data. The unambiguous velocity estimate is obtained by subtracting a single Nyquist interval of 4.2 ms^{-1} from the value obtained in (*A*) and two Nyquist intervals (or −8.4 ms^{-1}) from the value displayed in (*B*).

Discussion

The complete lack of smaller streak drops in the B2 grouping shown in Fig. 5 was an unexpected result of the initial analysis, and ended up serving as the primary motivation for examining the possible role of other factors in differentiating which particles the MCR detected as streaks. While microphysical arguments could possibly be invoked to explain the lack of larger particles in the gap region containing the B1 analysis domain, it would seem highly unlikely that particles less than 2 mm were entirely absent near the stronger rain shaft entering B2 evident in Fig. 1. This is supported by the in situ aircraft data aloft (Fig. 1) and the presence of the broad background reflectivity values generally in excess of 0 dBZ that are observed to flank the primary B2 rain shaft (Fig. 3). What then leads to the utter lack of individual streaks below the 2 mm threshold in the B2 analysis domain?

For clues, we plot the solutions for the particle diameter obtained from Eq. **1***A* for a wide variety of SIR and background

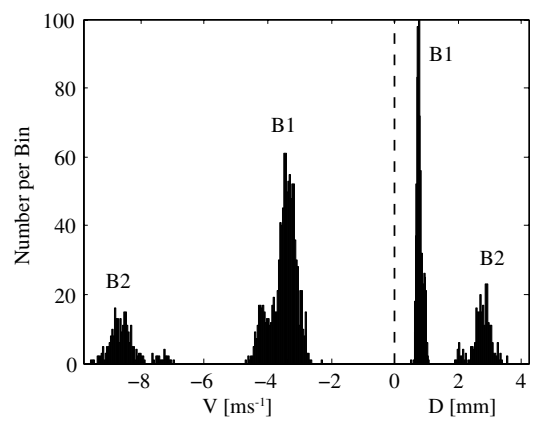

Fig. 5. Histograms of velocity (ms^{-1}; *Left*) and particle diameter (mm; *Right*) derived from the observed streak slopes. The B1 and B2 labels refer to the two main streak groupings discussed in the text. The velocity values are derived directly from the digitized streak slopes (see *Text*), while the diameters are derived from application of the velocity-diameter relationship of (17). The velocity bin size is 0.05 ms^{-1}, while that for diameter is 0.02 mm.

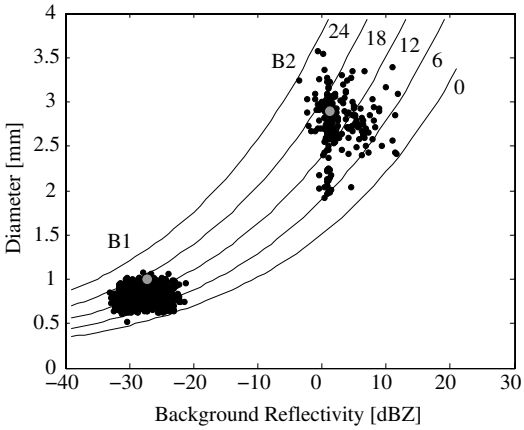

Fig. 6. Curves derived from Eq. **1***A* showing the theoretical minimum detectable drop diameter (mm) as a function of the background reflectivity (dBZ) and various values of SIR (labeled in dB). The plotted solid circles represent the calculated diameter and background reflectivity of each streak. The diameter was computed by the slope method while the computation of the background reflectivity value was derived from a power-weighted average of the reflectivity obtained from nearby range gates residing on either flank of the streak. The labels B1 and B2 refer to the two main streak groupings discussed in the text. The gray dots depicted in the B1 and B2 groupings denote the location of the S1 and S2 streaks, respectively.

reflectivity values (Fig. 6). The plotted curves show a number of interesting features which highlight the role of the background reflectivity in determining which particles stand out as streaks in the MCR time-height plots. First note that the curves confirm the expectation that larger particles serve as the streaks in the face of an increasing background reflectivity field. Note also that the spread in detectable diameters between any two SIR limits also increases with the background reflectivity suggesting, in general agreement with the plotted data shown in the histograms of Fig. 5, that a wider size distribution of particles may be expected in environments that have a higher background reflectivity.

The plotted data points represent the derived streak diameter and background reflectivity values obtained for each streak grouping. The streak diameter was determined from the slope method, while the background reflectivity value was obtained by computing an average power-weighted reflectivity value from a limited number of surrounding range gates lying beyond a five-gate offset from the immediate streak axis. The plotted data points are found to be in excellent agreement with the plotted theoretical curves. They also reveal that a well-defined lower limit in the SIR of approximately 6 dB is required before the particles stand out as streaks against a given background reflectivity. Thus, even though the MCR can detect a single particle of 273 μm at a range of 2 km with no background reflectivity, in practice the background reflectivity adds an additional factor $(\mathrm{ZNR}+1)^{1/6}$ [see Eq. **1***A*] which acts to increase this limit to the ~600 μm limit evident in Fig. 6.

The main results illustrated above suggest that a combined use of two waveforms, such as available with the MCR, allows both the bulk cloud structure and individual particle properties to be ascertained at the same time. Similar to the traces left behind on film by subatomic particles, larger cloud particles were observed to leave behind a well-defined signature (or streak) on the background radar reflectivity time-height field which could subsequently be used to infer their underlying properties. The single particle interpretation is supported by the excellent agreement found between three independent estimates, which were used to derive the particle diameter and velocity. We anticipate that these unique high-resolution radar data sets will lead to increased understanding of the internal structure and cloud dynamics that have long served the development of cloud microphysical parameterizations utilized in both cloud resolving and climate prediction systems.

Methods

We analyze the streaks by assuming that they represent a single dominant rain drop passing through a weaker background reflectivity comprised of much smaller particles. The case in which the streaks possibly represent a cluster of two or more dominant drops has been determined to have an exceedingly low probability of occurrence in the low precipitation environments examined here, and is not addressed further in this initial study. Since the MCR is calibrated with a weather radar equation that actually assumes that backscatter follows the Rayleigh approximation, and that the complete volume is filled with particles, the reflectivity factor, Z, may be directly used to calculate the diameter (D) via:

$$D = \{R^2 V_1 Z\}^{\frac{1}{6}}. \qquad [2]$$

In Eq. **2** R is the range (km) and V_1 ($\mathrm{m}^3/\mathrm{km}^2$) is the range normalized volume, which at a range of 2 km is 14.18 cubic meters. In applying Eq. **2**, the underlying assumption is that the smaller background precipitation particles contained within the pulse volume contribute insignificantly to the back scatter when compared to the single larger drop that causes the streak. The parameter values needed to evaluate Eq. **2** are extracted along a given streak axis at each radar pulse that intersects the streak. Once an estimate of D is obtained for each pulse, the velocity-diameter relationships of (17) are then used to compute the velocity such as is shown in Fig. S4. The average value of the diameter is estimated by performing a power-weighted average of the 256 reflectivity estimates shown in Fig. S4 and is listed in Table S1.

A second independent method of determining the streak diameter was computed from the slope of each discernible streak, such as is evident in the raw wideband time-height plots shown in Figs. 2 and 3. The slope was calculated by digitizing the starting and ending locations of each streak using the Getdatagraphdigitizer software and then computing the ratio of the resulting range and time increments. As the slope of each streak in a time-height plot can be directly related to a drop's total vertical velocity ($V = V_T + w$), estimates of the particle's diameter can be made provided the ambient vertical velocity (w) is small (shown to be a good approximation) in comparison to the terminal velocity (V_T) of the drop in question. As the drops that produce the streaks examined here are conveniently found to reside in the upper two size categories considered by (17) [Regime2: 20 μm < D < 1.07 mm and Regime3: 1.07 mm < D < 7.0 mm], we use the diameter-velocity relationships for those two size regimes exclusively to numerically determine the diameter listed in Table S1 from a given estimate of V_T obtained from the slope method.

One final independent estimate of the particle diameter can be derived from an estimate of the particle's velocity obtained from an analysis of the particle's Doppler phase shift (16). The algorithm for extracting the vertical velocity from the MCR data proceeds in standard fashion by computing the FFT of the complex signal voltage formed from the in-phase and quadrature signal components and constructing the corresponding power spectra. As is the case in the application of Eq. **2**, the FFT is constructed from the reflectivity and phase data extracted along the streak axis. The FFT for each streak was constructed from the 256-point data sample plotted in Fig. S4. As with the slope method, the velocity-diameter relationships of (17) are then applied to estimate the particle diameter listed in Table S1.

ACKNOWLEDGMENTS. These measurements were supported under grants N0017810WX00380 and N0003010RC1083R from the Naval Surface Warfare Center Dahlgren Division. D.B.B. was supported in part by the ONR NICOP grant to the University of Warsaw. We also gratefully acknowledge the support received from the Cape Canaveral Air Force Station Facility site MET Manager for balloon launches (Dave Chapman), the NASA Space Shuttle Program Manager (Dr. William Parsons), the NASA Debris Radar Project Manager (Anthony Griffith), the Naval Ordnance Test Unit Chief Engineer (Dr. Sid Beck), and Mr. Edward Powell. Additional support was provided by Mr. Hank Tracy of the Federal Aviation Administration and other air traffic controllers responsible for guiding aircraft in the Cape Canaveral, FL region. Stephen Schindler and William Trammell helped secure radiation permission for the ground-based Micro Rain Radar. Mr. Kim Richardson, Mr. John Cook, Mr John Kopp, and Mr. Mark Brunges of the Naval Research Laboratory helped furnish real-time model satellite data sets and provided logistical support with all our equipment. Mr. Chuck Deming of IEC Corp aided in the processing of data from the MCR radar data and its operation. The late Dr. Julius Goldhirsh of the Johns Hopkins University Applied Physics Laboratory is recognized for laying down the MCR weather measurement foundations upon which this study was ultimately based. The authors are grateful for the comments and suggestions received by two anonymous reviewers, which led to improvements in the text.

1. Stephens G-L (2005) Cloud feedbacks in the climate system: A critical review. *J Climate* 18:237–273.
2. Stephens G-L (1994) *Remote sensing of the lower atmosphere: An introduction* (Oxford Univ Press, New York).
3. Cess R-D, et al. (1990) Intercomparisons and interpretation of climate feedback processes in 19 atmospheric general circulation models. *J Geophys Res* 95:16601–16615.
4. Senior C-A, Mitchell J-F-B (1993) Carbon dioxide and climate: The impact of cloud parameterization. *J Climate* 6:393–418.
5. Smith R-N-B (1990) A scheme for predicting layer clouds and their water contents in a general circulation model. *Quart J Roy Meteor Soc* 116:435–460.
6. Miller S-D, Stephens G-L, Beljaars A-C-M (1999) A validation survey of the ECMWF prognostic cloud scheme using LITE. *Geophys Res Lett* 26:1417–1420.
7. Meehl G-A, Boer G-J, Covey C, Latif M, Stouffer R-J (2000) The Coupled Model Intercomparison Project (CMIP). *Bull Amer Meteor Soc* 81:313–318.
8. Colman R, Fraser J-R, Rotstayn L (2001) Climate feedbacks in a general circulation model incorporating prognostic clouds. *Climate Dyn* 18:103–122.
9. Hogan R-J, Jakob C, Illingworth A-J (2001) Comparison of ECMWF winter-season cloud fraction with radar-derived values. *J Appl Meteor* 40:513–525.
10. Randall D-A, Khairoutdinov M, Arakawa A, Grabowski W (2003) Breaking the cloud parameterization deadlock. *Bull Amer Meteor Soc* 84:1547–1564.
11. Webb M-J, Senior C, Bony S, Morcrette J-J (2001) Combining ERBE and ISCCP data to assess clouds in the Hadley Centre, ECMWF, and LMD atmospheric climate models. *Climate Dyn* 17:905–922.
12. Brook M, Latham D-J (1968) Fluctuating radar echo: Modulation by vibrating drops. *J Geophys Res* 73:7137–7144.
13. Musgrove C, Brook M (1975) Microwave echo fluctuations produced by vibrating water drops. *J Atmos Sci* 32:2001–2007.
14. Atlas D, Harper W-G, Ludlam F-H, Macklin W-C (1960) Radar scatter by large rain. *Quart J Roy Meteor Soc* 86:468–482.
15. Beard K-V, Kubesh R-J (1991) Laboratory measurements of small raindrop distortion. Part 2: Oscillation frequencies and modes. *J Atmos Sci* 48:2245–2264.
16. Doviak R-J, Zrnic D-S (1984) *Doppler radar and weather observations* (Dover, Mineola, NY), pp 89–97.
17. Beard K-V (1976) Terminal velocity and shape of cloud and precipitation drops aloft. *J Atmos Sci* 33:851–864.
18. Beard K-V, Pruppacher H-R (1971) Wind tunnel investigation of the rate of evaporation of small water drops falling at terminal velocity in air. *J Atmos Sci* 28:1455–1464.
19. Li X, Srivastava R-C (2001) An analytical solution for raindrop evaporation and its application to radar rainfall measurements. *J Appl Met* 40:1607–1616.
20. Hildebrand P-H, Sekhon R-S (1974) Objective determination of noise-level in Doppler spectra. *J Appl Met* 13:808–811.
21. Rayleigh J-W-S (1879) On the capillary phenomena of jets. *Proc R Soc London* 19:71–97.
22. Gunn R (1949) Mechanical resonance in freely falling raindrops. *J Geophys Res* 54:383–385.
23. Szakall M, Mitra S-K, Diehl K, Borrmann S (2010) Shapes and oscillations of falling raindrops—A review. *Atmos Res* 97:416–425.
24. Pruppacher H-R, Klett J-D (1978) *Microphysics of Clouds and Precipitation* (Reidel, Boston, Massachusetts), pp 322–326.